



HAL
open science

A promising method to derive the temperature coefficients of material constants of SAW and BAW materials. first application to LGS

Pascal Nicolay, Thierry Aubert

► **To cite this version:**

Pascal Nicolay, Thierry Aubert. A promising method to derive the temperature coefficients of material constants of SAW and BAW materials. first application to LGS. IEEE Transactions on Ultrasonics, Ferroelectrics and Frequency Control, 2014, 61 (8), pp.1335-1343. 10.1109/TUFFc.2014.3041 . hal-01257415

HAL Id: hal-01257415

<https://hal.science/hal-01257415>

Submitted on 24 Feb 2023

HAL is a multi-disciplinary open access archive for the deposit and dissemination of scientific research documents, whether they are published or not. The documents may come from teaching and research institutions in France or abroad, or from public or private research centers.

L'archive ouverte pluridisciplinaire **HAL**, est destinée au dépôt et à la diffusion de documents scientifiques de niveau recherche, publiés ou non, émanant des établissements d'enseignement et de recherche français ou étrangers, des laboratoires publics ou privés.

A promising method to derive the temperature coefficients of material constants of SAW and BAW materials. First application to LGS.

Pascal Nicolay¹, Thierry AUBERT²

¹ Carinthian Tech Research, Villach/St. Magdalen, Austria

² Laboratoire SYMME, Université de Savoie, Annecy-le-Vieux, France

Abstract — LGS is a promising material for SAW applications at high temperature. However, the temperature coefficients of LGS material constants are not accurate enough to perform reliable simulations and therefore to make good use of available design tools above 300°C. In the first part of the paper, we describe a new possible way to derive these coefficients in a wider temperature range. The method is based on Simulated Annealing, a well-known optimization algorithm. The algorithm converges towards a set of optimized temperature coefficients of the stiffness constants which are used to perform accurate simulations up to at least 800°C. In the second part, a deeper analysis of the algorithm outputs demonstrates some of its strengths but also some its main limitations. Possible solutions are described to predict then improve the accuracy of the optimized coefficient values. In particular, one solution making use of additional BAW target curves is tested. A promising solution to extend the optimization to the temperature coefficients of piezoelectric constants is also discussed.

Keywords- LGS; temperature coefficients; high temperature; optimization; Simulated Annealing; Rayleigh modes

I. INTRODUCTION

The design of high-temperature Surface Acoustic Wave (SAW) sensors requires prior knowledge of the first and second order temperature coefficients of the substrate material constants (TC1 and TC2). However, direct measurement of material constants is very challenging at high temperature. Concerning LGS which is one of the most promising SAW substrates for high temperature applications, available TC1

and TC2 sets are reliable up to 300°C at best [1]. Therefore, it is not possible to perform accurate predictions above this temperature.

If direct characterization of material constants is difficult to achieve, indirect determination might be a good solution. For instance, acoustic waves of various kinds can be used to probe the material and extract the needed information. Indeed, changes in velocity and therefore velocity-related parameters (frequency, time delay, phase...) depend directly on the TC1 and TC2 coefficients. This approach is becoming more and more appealing as recent technical achievements made it possible to characterize SAW properties up to at least 900°C [2-3]. In this case, one possible way to perform the extraction is a curve fitting procedure. The SAW properties are simulated first in a wide temperature range then the TC1 and TC2 used in the simulation are adjusted ('optimized') to fit the computed results to the experimental data ('target curves').

The first difficulty of the optimization procedure is that many coefficients are involved and must be simultaneously tuned. For the stiffness coefficients of LGS alone, twelve coefficients must be considered (six TC1 and six TC2). If the TC1 and TC2 of the piezoelectric constants and expansion coefficients are to be considered too, this number rises to twenty. To fit adequately these coefficients, we would need at least an equal number of 'non-correlated' experimental curves. By 'non-correlated' curves, we mean experimental curves with different dependency patterns on the various parameters to be optimized. It is necessary to use non-correlated curves to converge towards the best solution (i.e. the best set of TC1 and TC2 coefficients) the same way as it is necessary to use N non-correlated equations to solve a system of linear equations with N unknown values. Non-correlated curves can notably be obtained using different cuts, different propagation directions or different wave modes. Additionally, a given coefficient will be well optimized only if several of the non-correlated target curves share a strong dependence on it. For instance, if none of the required target curves depends strongly on C11, it won't be possible to optimize this coefficient or at least not with a good enough accuracy. If only one curve depends strongly on C11, the optimization will be improved (especially if the curve depends solely on C11) but it won't be possible to benefit from the global optimization process to improve the fitting accuracy on C11. That is, C11 will be

obtained from one curve only which implies a rather poor accuracy due the measurement uncertainties on the target curve itself. If two or more non-correlated target curves share a strong dependency on C11, the optimization process will improve the accuracy. Indeed, each of the curves will define a given range of possible values for C11 (i.e. the error bar around the calculated value) but all of these possible ranges will only overlap in a much smaller region, delimiting the actual and much improved range of possible values for C11. This feature of a system of target curves will be called ‘multiplicity’ in the following chapters. Following this rather intuitive analysis, it appears that a set of coefficients will be well optimized only if enough ‘non-correlated’ target curves are available, with several of them sharing a strong dependence on each of the coefficients. This will serve as a guideline in the following chapters, where solutions to improve the performances of the optimizer as well as the accuracy of the obtained LGS coefficients will be discussed. This also makes it clear that if only a handful of target curves are available, the optimization process won’t yield a complete set of accurate optimized coefficients. Several distinct TC1 and TC2 sets might even emerge as possible solutions to the fitting procedure. However, there are still ways to obtain good results in this case. As will be shown in the next chapters, a good way to avoid converging towards a wrong solution might be first to reduce the number of variables and second, to start from a solution that is already as close as possible to the optimum. The latter implies looking first for the best possible set of available coefficients then use it as a starting point for the optimization.

Besides, it is also very important to select target data that were not (or as little as possible) influenced by parameters other than the ones taken into account in the simulations. For instance, if SAW curves are used as target, it is important to use data obtained with very thin IDTs. Indeed, thicker IDTs have a clear influence on the Fractional Frequency Changes (FFC) curves, especially at high temperature or for very sensitive wave modes and orientations. This was shown for instance for Pt IDTs on LGS, which have been experimentally investigated on the orientations $(0^\circ, 138.5^\circ, 26.6^\circ)$ and $(0^\circ, 22^\circ, 31^\circ)$ up to 700°C . Big discrepancies between the frequency-temperature laws for devices made with different Pt relative thicknesses were observed, in particular on the $(0^\circ, 22^\circ, 31^\circ)$ orientation. First simulations show that this

phenomenon could be at least partly related to large thermoelastic effects occurring in Pt electrodes at high temperature when the temperature rises [4].

The second difficulty of the fitting procedure is the optimization phase itself. If twelve to twenty coefficients have to be considered simultaneously, it is not reasonable to test all of the possible combinations to ultimately choose the best one. This would consume way too much time. A search algorithm has to be used instead. A promising solution is the Simulated Annealing (SA) algorithm which is well known for its ability to find the global minimum of a multivariable function [5].

The approach described above has been tested first on LGS using FFC target curves on three distinct cuts – (0°, 22°, 31°), (0°, 90°, 0°) and (0°, 138.5°, 26.6°) – and a full set of starting constants and associated TCs extracted from [6] and [7]. The optimization was performed on the six TC1 and six TC2 of the stiffness constants only. This means that the stiffness constants themselves (i.e. C_{ij} at room temperature) were not optimized and therefore kept constant all along the procedure.

The optimized coefficients have been subsequently used to successfully predict the FFCs of two test cuts – (0°, 144°, 24°), (0°, 22°, 90°) – in a wide temperature range (up to 800°C) [8]. It is stressed that these two test cuts were not taken into account during the optimization process. They were used afterwards to check the ‘quality’ of the optimized set of TCs. The constants and optimized coefficients are presented in Table I.

TAB. I. LGS STIFFNESS CONSTANTS [6] AND OPTIMIZED TC [8]

	Constant @ 20°C $10^{10} \text{ [N/m}^2\text{]}$	TC1(ppm/°C)	TC2(ppb/°C²)
C11	18.89	-65	-39
C33	26.83	-105	-55
C44	5.33	-63	-80
C66	4.237	-29	-23
C13	10.15	-84	-86
C14	1.442	-304	88

The main goals of the present paper are first to explain in more details the inner-working of the optimizer and provide a thorough analysis of the obtained results, second to expose the limitations of the method, third to provide solutions to improve the quality of the results (i.e. the accuracy of the optimized coefficients).

The complete optimization algorithm, including preparation steps, is presented in chapter 2. The main optimization parameters are described. The results of four optimization runs are compared. The convergences towards a minimal error follow very similar tracks and provide fitting curves of the same quality. However, if all the runs do converge towards the same solution for some of the coefficients, the dispersion for other coefficients is quite high. This constitutes a first limitation of the procedure. In chapter 3, we analyze the reasons for the dispersion and show that the dispersed coefficients were not optimized at all. We provide a simple procedure and graphic tool to support the analysis and predict which coefficients are going to be well optimized and which are not. A solution to minimize the dispersion is suggested, discussed and tested. It combines acoustic measurements of different kinds (SAW and BAW). In chapter 4, we check the algorithm's ability to converge towards the optimum solution when starting from a distant initial solution, built out of published data. It is shown that the algorithm does not converge towards the best optimum in that case, which constitutes a further limitation of the procedure. Complementary test results show that in the particular configuration used to derive the coefficients of Table I that is with the three already-mentioned SAW curves as target, the optimizer is able to re-converge towards the best identified solution as long as the 'measurement error' on the various coefficients (i.e. the differences between the starting values and the optimized values from Table I) is kept below a given limit. Beyond this limit, the optimizer starts converging towards alternative solutions. This definitely validates the capability of the optimizer to find a solution from any starting point. It also confirms that a well-defined and complete set of target curves must be used to ensure that the optimizer finds the right solution (i.e. TCs 'equal' to the natural ones). If such a set is not available, the optimizer will converge towards the right solution only if the starting point is not located too far from it. In chapter 5, an updated procedure is suggested to overcome

the limitations presented before. We also propose to add complementary calculation modules to optimize the TCs of the piezoelectric constants. This module would make use of other kind of experimental measurements and simulation methods to compute the error to minimize.

II. THE OPTIMIZATION PROCEDURE

A. The method

The complete procedure is sketched in Fig. 1. First, FFC curves are retrieved in the literature for as many cuts as possible, as well as sets of material constants and coefficients. A simulation tool is used to compute the FFC(s) for each set as well as combinations of subparts of sets. This allows for selecting the best starting set of parameters (\mathbf{X}_0) and computing a starting error value Z_0 . Then, the parameters to be optimized are chosen (we chose to perform the optimization on the TC1 and TC2 of the stiffness constants only). The optimization procedure starts with the pseudo-random generation of a new set of parameters (\mathbf{X}) ‘around’ \mathbf{X}_0 . In our case, the new set was generated using the Matlab `randn(n)` function, which draws values from the standard normal distribution. The chosen standard deviation was 0.5ppm/K for TC1 and 2.5ppb/K² for TC2. The FFC(s) are then computed for each of the selected curves and a new error Z is calculated. In the next step, Z is compared to Z_0 . If Z is smaller than Z_0 , the old ‘best’ set is replaced by the new one and a new cycle begins. If Z is bigger than Z_0 , the decision of acceptance or refusal of the new solution is based on the Metropolis criterion [5]. This criterion makes the acceptance of the new (worse) solution all the more likely than ‘temperature’ is high and $Z-Z_0$ is small. ‘Temperature’ is used here to describe a parameter that steadily decreases with time, over the whole optimization process. The term ‘temperature’ was chosen by analogy with the physical process of thermal annealing, which is mimicked by the SA algorithm. The ‘temperature’ is lowered over time, which progressively decreases the probability to accept a worse solution. The strength of the SA algorithm precisely resides in its ability to keep exploring worse solutions to avoid being stuck in local minima. The optimization stops when the error cannot be further reduced. Concerning the simulation tool, it is chosen with respect to the modes that

have to be computed (SAW, BAW, LSAW, etc...). In our case, we selected target FFC curves involving only Rayleigh modes. To compute these modes, we used a self-made tool based on the well-known Campbell and Jones method [9].

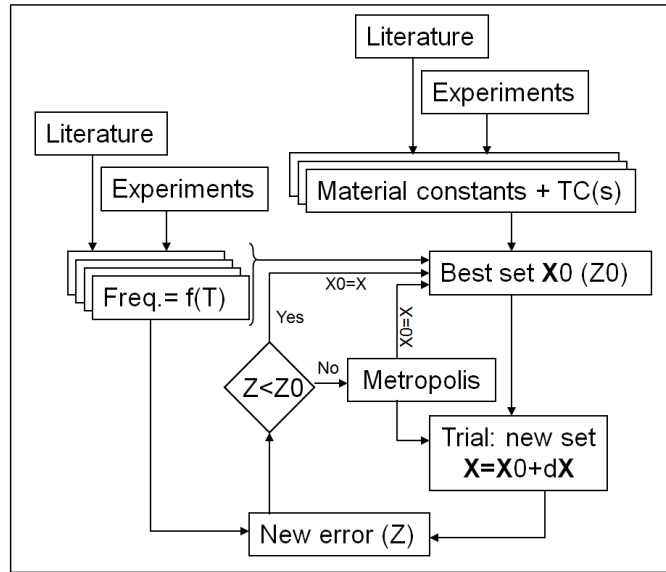


Fig. 1. The optimization procedure.

B. The results

Four optimizations were performed on a Fujitsu desktop computer (3.3GHz CPU, 4GB RAM). Each run took approximately 24 hours for an average of 2500 iterations. The starting solution and optimization parameters were identical to the ones described in [8]. Only the standard deviation (σ) was different (five times bigger). All the convergence patterns (including the reference pattern published in [8]) are presented in Fig. 2. The patterns are all very similar and converge towards the same minimum value (~ 0.35). However, it is clear that a bigger σ allowed for a significant decrease in convergence time.

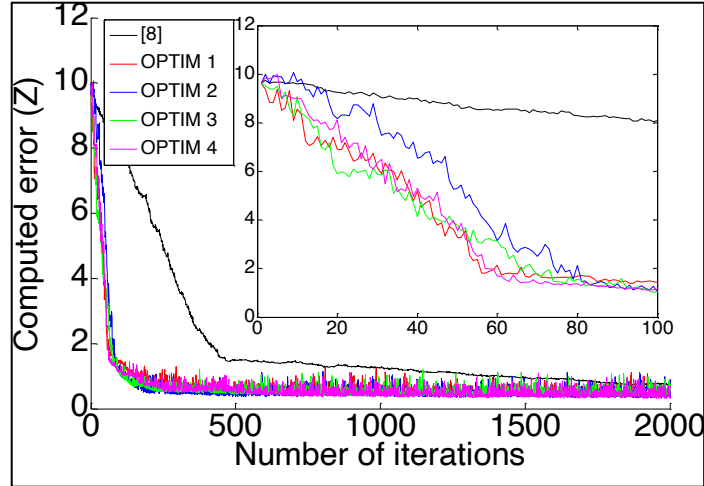


Fig. 2. Error evolution vs. iteration during optimization process. Inset: zoom on the first 100 iterations.

The FFC(s) obtained with each of the four optimized sets of coefficients are presented in Fig. 3, for two of the target curves. The ‘fitting quality’ is just as good in each case. The FFC of the $(0^\circ, 90^\circ, 0^\circ)$ cut is not represented here for clarity reasons, the FFC(s) of the $(0^\circ, 22^\circ, 31^\circ)$ and $(0^\circ, 90^\circ, 0^\circ)$ cuts being almost identical. Finally, the variations of the TC values before and after optimization are presented in Fig. 4, for each of the runs. First, it can be seen that some coefficients ‘moved’ more than others. Second, it appears that the optimization results are very close to each other for some of the coefficients (C66, C44) but strongly dispersed for others (C11, C13). This is an important result which demonstrates one of the main limitations of the optimization procedure. Indeed, if several distinct values can be obtained for some of the coefficients, these values just cannot be trusted.

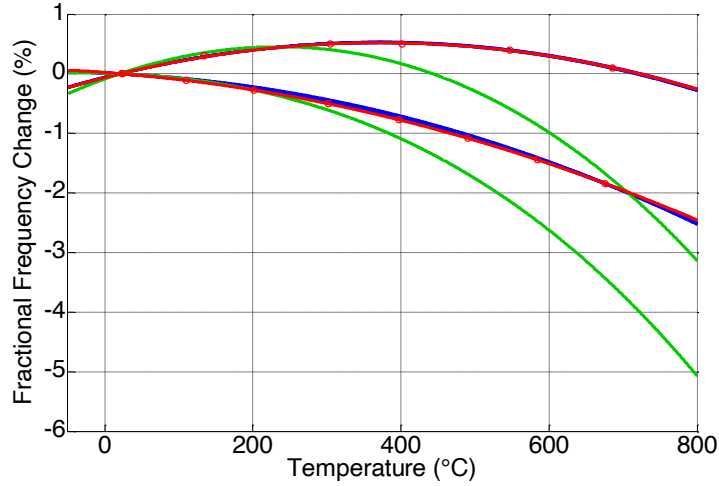


Fig. 3. Starting point (green) and optimization result (blue) on distinct experimental LGS Target Curves (red). Above – (0°,22°,31°); below – (0°,138.5°,26.6°).

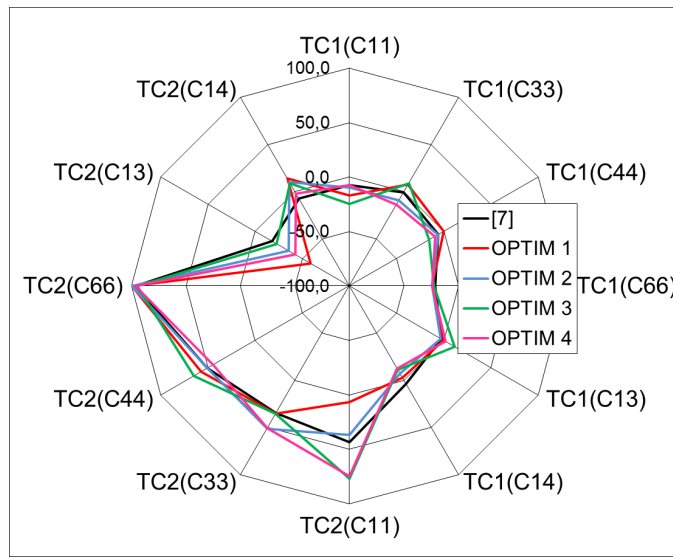


Fig. 4. (TC_final-TC_initial) for each of the optimized coefficients. The scale is in ppm/K for TC1 and ppb/K² for TC2 values.

III. RESULTS ANALYSIS

The reason for the observed dispersion is that the Rayleigh modes propagating on the three target cuts depend very little on the coefficients C11, C33 and C13. The dispersion is due to the stochastic exploration of the solution space for these constants. The ‘optimized’ TC1 and TC2 for these constants result from Brownian motions around the starting values (see Fig. 5). However, the very accurate

prediction of the SAW behavior on two test cuts as reported in [8] show that the optimized values C66, C44 and C14 probably can be trusted. The predictions were good because the observed modes do not significantly depend on C11, C33 and C13 for these two cuts.

A sensitivity map for the three target curves is presented in Fig. 6. The sensitivity of the error Z to the variation of each of the twelve coefficients TC1 and TC2 is quantified for each of the target curves. The plotted values correspond to the Z variation for a change of +1ppm/K for TC1 and +1ppb/K² for TC2 values. We can see that the error depends strongly on C66, quite a lot on C44 and C14 and only very little on C11, C33 and C13, for each of the represented curves.

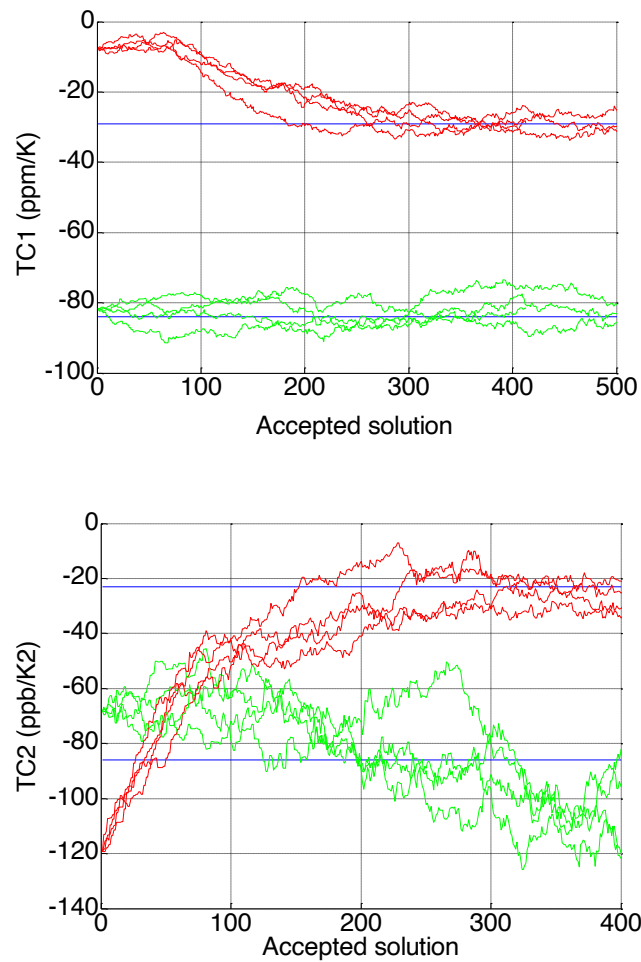


Fig. 5. Convergence paths for C66 (red) and C13 (green). Top: TC1 values; bottom: TC2 values. 'Accepted solution' refers to the number of new sets (**X**) accepted as solutions by the SA algorithm, during the optimization.

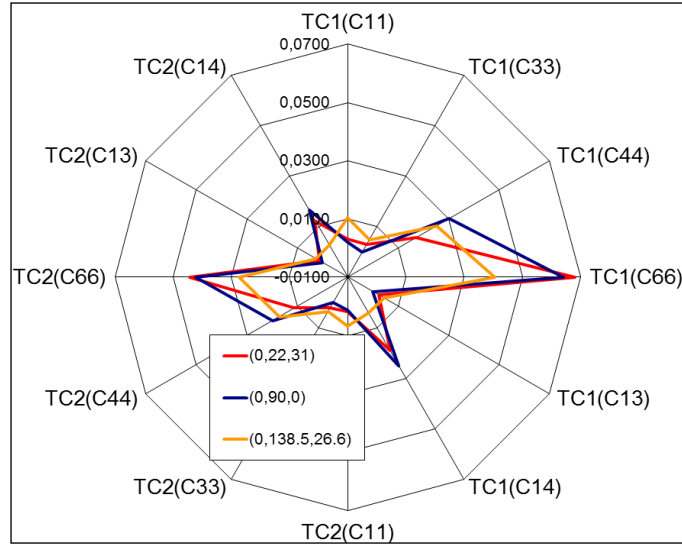


Fig. 6. Sensitivity map. Effect (ΔZ) of a +1ppm/K (+1ppb/K²) change of TC1 (TC2) values on the computed error Z.

Moreover the three profiles are similar which makes the three target curves rather poorly complementary to each other. The sensitivity map is a useful tool to start with prior to the optimization. It makes it possible to visualize and estimate the two important features described in the Introduction section which are the degrees of correlation (how different are the sensitivity patterns?) and multiplicity (how many target curves do I have showing a strong sensitivity on a given coefficient?). To ensure that all of the chosen coefficients will be optimized, the area(s) enclosed by the sensitivity polygons must be maximized and the polygon shapes must differ as much as possible from one target curve to the other.

In the present case, the three target curves appear to be correlated and global multiplicity is bad (there is no sensitive target curve for C11, C33 and C13) with the consequence that C11, C33 and C13 cannot be well optimized. Another consequence is that the starting point has to be close to the optimum in order to optimize with a good-enough accuracy the three other coefficients. Indeed, a high degree of correlation makes it easier to converge towards alternative solutions (by analogy, if a complete system of linear equations comprises two identical equations, the number of solutions becomes infinite). However, if the starting point is close to the global minimum, we can still hope finding it and this is probably what happened here.

More non-correlated target curves with higher multiplicity on C11, C33 and C13 are obviously

needed to optimize these coefficients. The first possibility would be to look for specific cuts and propagation directions whose Rayleigh modes would depend mainly on these constants. But BAW measurements could be simpler to use and very practical. Longitudinal BAW modes (L-BAW) in the directions X (1,0,0) and Z (0,0,1) are respectively dependent on C11 only and C33 only. Using these two directions plus one additional direction (1,0,1) to increase the overall dependency on C13 would yield the sensitivity map presented in Fig. 7. The sum of the individual sensitivity plots is represented in Fig. 8, before and after consideration of the additional three L-BAW modes. When the three L-BAW modes are included, all of the TCs have a non-negligible effect on the global error which is mandatory for the optimization. However, it appears that C13 is still a weak point in this configuration. It is not the purpose of this work to find the best possible configurations to ensure the best possible optimization but this is clearly a very important issue that will have to be addressed in future work. The goal will be to define the minimum number of cuts, orientations and wave-modes (including SH-SAW, pseudo-SAW, SH-BAW, Lamb modes etc...) to characterize in order to ensure an as perfect as possible convergence towards the best possible TCs values.

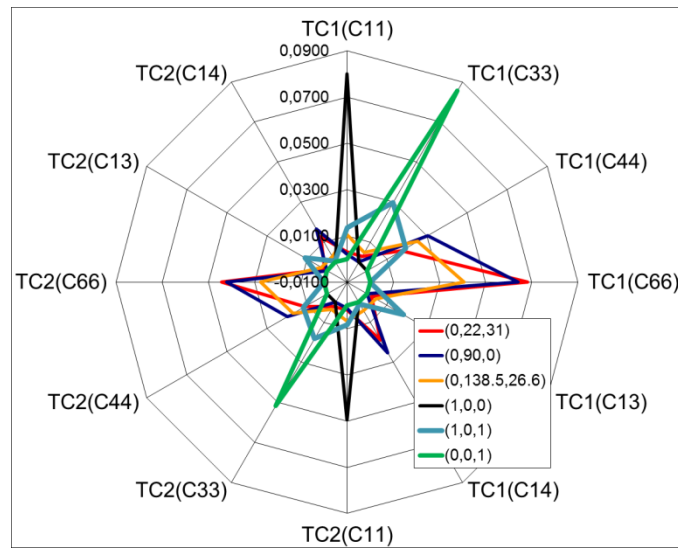


Fig. 7. Sensitivity map, with SAW and L-BAW target curves.

Effect (ΔZ) of a +1ppm/K (+1ppb/K²) change of TC1 (TC2) values on the computed error Z.

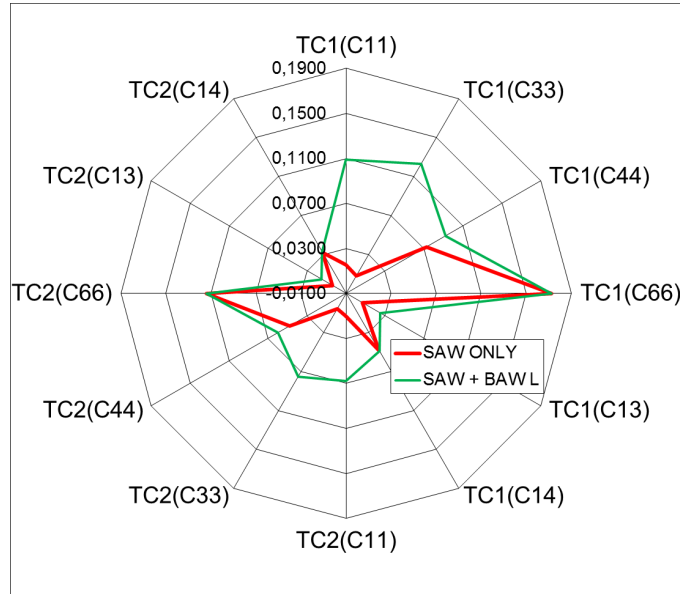


Fig. 8. Global Sensitivity maps with (green) and without (red) L-BAWL targets.

As a first step in this direction, the configuration described in Fig. 7 and 8 was tested. The simulation tool was upgraded to simulate longitudinal and transverse BAW modes. We were not able to find the required target curves in the literature. Therefore, we created them manually, from scratch. That is, we generated parabolic curves without any physical sense, our goal being only to check the convergence pattern of the optimizer in the new configuration described above (i.e. 6 target curves). The convergence patterns for C11, C33 and C13 are showed in Fig. 9, for TC1 and TC2. In each case, the evolution follows a well-defined path which confirms that all of the coefficients are being actually optimized. This is a promising result which confirms the interest of the method although improvements and further testing are still required.

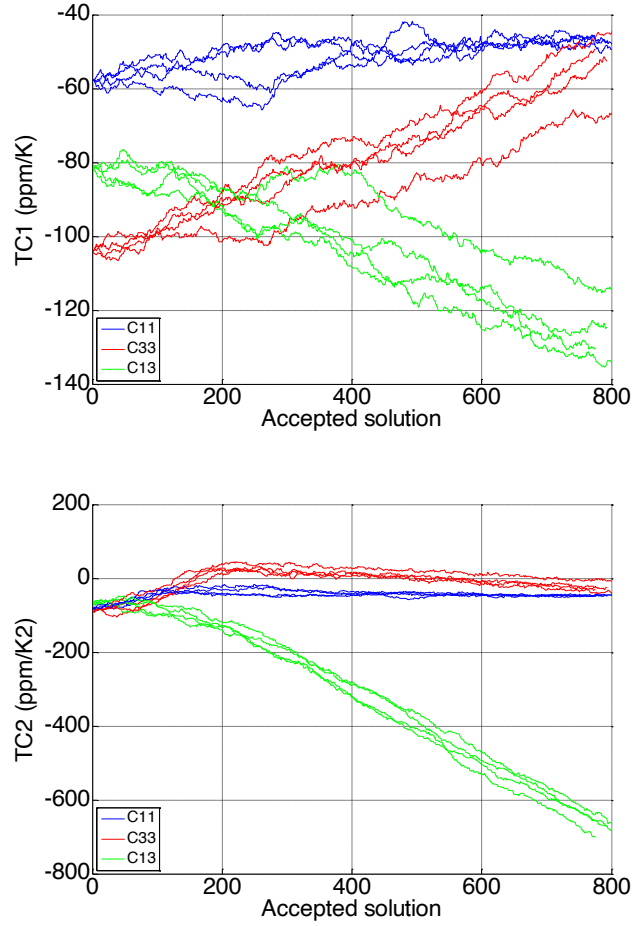


Fig. 9. Convergence patterns for C11, C33 and C31 when L-BAW and SAW curves are used as targets. Well-defined convergence patterns are visible for each of the coefficients. Top: TC1 values; bottom: TC2 values.

IV. ALGORITHM 'ROBUSTNESS'

In the previous section, we showed that the algorithm optimizes all of the parameters when provided with an adequate set of target curves. Besides, it is also interesting to evaluate the algorithm's ability to converge towards the global optimum when starting from a more distant set of parameters. In other words, we would like to check if the optimizer still retrieves the values from Table I when starting from a very different set of values. To perform this complementary study, we first used starting constants and coefficients from [10]. The results of the optimization run (1740 iterations, standard deviation parameters: 0.5ppm/K for TC1 and 2.5ppb/K² for TC2) are presented in Fig. 10. The target curves were

again (0°, 22°, 31°), (0°, 90°, 0°) and (0°, 138.5°, 26.6°). No ‘dummy’ BAW targets were used here. The algorithm did converge towards a lower error ($Z=1.06$) but the results were not satisfying. The algorithm got stuck in a local minimum and did not manage to evolve towards a better solution. To allow the algorithm for finding a better solution, the optimization was re-run with increased excursion parameters. This yielded no better results. The maximum standard deviation parameters tested here were 50ppm/K for TC1 and 250ppb/K² for TC2. In this extreme case, no convergence occurred at all. The optimizer kept oscillating between huge error values, never managing to find any possible convergence way.

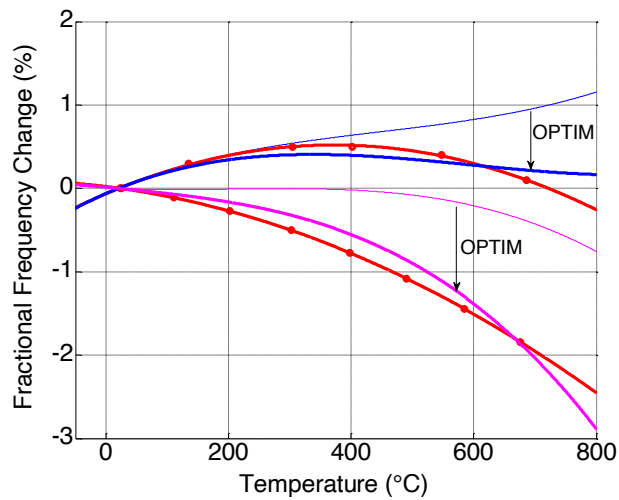


Fig. 10. Optimization from a distant starting point, for (0°, 22°, 31°) (above) and (0°, 138.5°, 26.6°) (below). Thin line(s): before optimization (using coefficients from [10]). Thick line(s): after optimization.

Nevertheless, even if the optimizer is unable to converge towards the correct solution when supplied with a too distant set of starting parameters, it is interesting to check the maximum distance until which it is still able to converge adequately. To perform the necessary calculations, we generated multiple sets of starting parameters with an increasing distance to the optimized coefficients presented in Table I. The starting sets were generated using the randn(n) function of Matlab to calculate random variations of each of the TCs prior to the optimization (i.e. $TC_initial(C_{ij}) = TC_TableI_ (C_{ij}) + random_number_ij$, where random_number_ij is obtained using the randn(n) Matlab function with a given standard deviation σ). Several sets were generated for a given standard deviation. The standard deviation was progressively

increased from 5 to 35. The optimizations were performed in the initial configuration, using only the three SAW curves as targets. It appeared that the optimizer managed to re-converge towards the optimum values from Table I (or very close ones) up to $\sigma \sim 15$. Above this value, it started to converge towards very different sets of parameters. However, the optimizer always managed to find sets of values which allowed for an almost perfect fit of the target and test curves, even for higher σ values. In Fig. 11, we can see four sets of parameters which were the start and end values of two distinct optimization runs. The first of these two runs was used to obtain the data published in Table I. These data constitute our reference set (green line). The starting values (i.e. the Bungo coefficients) are represented in red. The second run was performed with $\sigma = 35$. The corresponding starting values are indicated in magenta and the result of the optimization run in blue. A comparison between the red and magenta lines gives the distance between the two starting sets. By definition, this distance increases with σ . To improve the readability of the figure, the reference set was subtracted to the three other sets. Therefore, the reference set is a green horizontal line on the X axis. A blue line close to the green one would mean that the run converged again towards the data from Table I. As mentioned before, this was observed for optimizations performed with σ values smaller than 15 (see thin blue line in Fig. 11 for one example of optimized set obtained with $\sigma=5$). However, the blue line obtained for $\sigma=35$ is far from the green line, meaning that the optimizer converged towards a completely different set of TCs. In Fig. 12, we present the fits obtained at the end of the ‘ $\sigma = 35$ ’ optimization using this new set of TCs. The result is almost as good as what was obtained using the coefficients from Table I (see Fig. 3).

First of all, this confirms the ability of the optimizer to converge towards a consistent solution even if the starting values are very inaccurate. Second, this confirms that three correlated target curves are not enough to enable the optimizer for discriminating between equivalent neighboring solutions (local optimums) and therefore converge towards the global optimum. In our ‘ $\sigma=35$ ’ example, the starting point was far enough to prevent the optimizer from re-finding the best solution. This gives a first measure of the error that could be tolerated on the starting values to ensure that the optimizer will still find the right

solution when only a few correlated curves are used as targets. It is stressed that even if at least one completely different set of TCs did allow for fitting the target and test curves as well as the TCs from Table I, the latter still have to be considered the best ones (at least for C66, C44 and C14). Indeed, they were obtained using a much better starting set of TCs meaning that the optimizer started from a location that was close enough to the global optimum to find it.

All these results will serve as basis for deeper analysis and improvement of the method. They already indicate that an adequate set of target curves should allow the optimizer for retrieving the optimum values even if the measurements are not accurate. This would advocate in favor of the following and promising method to derive accurate TCs with much less effort than previously required: 1. Look in the literature for a complete set of constants at room temperature; 2. Perform quick and dirty measurements up to 900°C, according to a well-defined and customized experimental planning; 3. Use numerical optimization supported for instance by Simulated Annealing to derive the TCs with a good enough accuracy. The method might be dubbed ‘QDMO’, after Quick and Dirty Measurements plus Optimization.

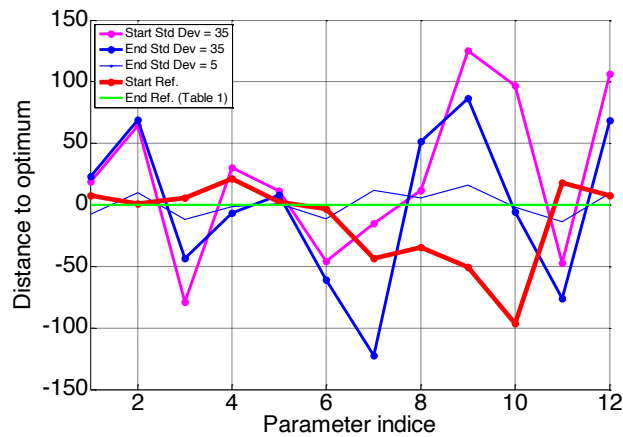


Fig. 11. Comparison Before/After Optimization for two runs with different starting sets of coefficients. The parameter indices correspond to the TC1s of C11(1), C33(2), C44(3), C66(4), C13(5), C14(6) and to the TC2s of C11(7), C33(8), C44(9), C66(10), C13(11), C14(12).

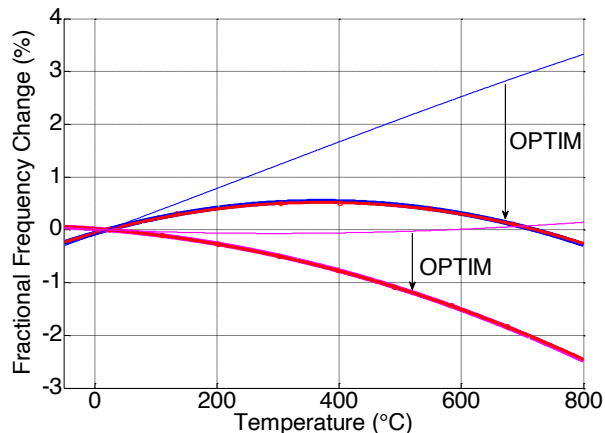


Fig. 12. Optimization from a distant starting point generated with $\sigma = 35$, for $(0^\circ, 22^\circ, 31^\circ)$ (above) and $(0^\circ, 138.5^\circ, 26.6^\circ)$ (below). Thin line(s): before optimization; Thick line(s): after optimization.

V. FUTURE STEPS

Considering the developments presented before, the first obvious step to improve the method will be to define the right set of target curves to be used to ensure that the optimizer always finds the global optimum or best set of TCs, whatever the starting point. Among others, this set will depend on the crystallographic structure.

A second point concerns the TCs of the piezoelectric constants. In essence, the QDMO method is based on complementary experimental results which are used together as a global target for an optimizer. The optimizer reduces the distance between experimental and numerical results by adjusting some pre-selected coefficients, therefore tuning them to what is hopefully their actual and natural value. If SAW and BAW measurements are certainly good choices to help tuning the TCs of the stiffness constants, another set of measurements could serve as good complementary targets to help tune simultaneously the TCs of the piezoelectric coefficients. Following the logic used before when L-BAW were suggested as good complements to help tuning C11 and C33, direct piezoelectric coefficient measurements might be used to help tuning e_{11} and e_{14} . A special piezoelectric module could be added to the calculation core of

the optimizer, allowing it to extract an error from the comparison between experimental and numerical results. A possible approach would be to use Laser Vibrometry characterization of piezoelectric materials, as described in [11]. In a few words, piezoelectric constants are extracted from (Laser-measured) vibration patterns using FEM computation to fit the numerical model to the experimental data. This could be advantageously implemented in the error calculation loop. Moreover, the non-contact nature of the measurement method (although electrodes still have to be used and bonded) makes this solution very attractive for high-temperature characterization.

Finally, it will be important to check the validity of the QDMO method against a set of accurate TCs determined in a more classical and direct way. The complete sets of constants and coefficients published recently for LGT [12] might very well constitute the perfect reference for testing the whole method. The goal will be to start from a small number of new SAW and BAW measurements (to be performed up to 900°C) then use SA Optimization to derive new TCs then compare these TCs to the published ones. If the difference is small, the validity of the QDMO method will be definitely confirmed.

VI. CONCLUSION

We showed that a SA algorithm coupled with a Rayleigh modes simulation tool might be used for accurate determination of temperature coefficients of material constants (LGS in the present case). The algorithm is able to fit experimental curves and extract the coefficients from the fitting results. However, we demonstrated that a complete optimization of all the coefficients of interest would require a bigger number of specific and non-correlated experimental plots. A graphic tool (sensitivity map) was suggested as a potential help to assess beforehand whether the optimization will actually converge towards a trustable solution for all of these coefficients or not. Future work will include looking for suitable complementary cuts and propagation modes to further optimize the whole set of TC1 and TC2 coefficients for LGS. The algorithm will also be used to extract optimized temperature coefficients for other potentially interesting substrates, including LGT.

VII. ACKNOWLEDGMENT

This work was partly funded within the COMET program, coordinated by the Austrian Research Promotion Agency (FFG).

REFERENCES

- [1] M. Weihnacht, A. Sotnikov, H. Schmidt, B. Wall and R. Grünwald, “Langasite: high temperature properties and SAW simulations,” in *Proc. IEEE Ultrasonics Symp.*, 2012, pp. 1549-1552.
- [2] M. Pereira da Cunha, R. J. Lad, T. Moonlight, S. Moulzolf, A. Canabal, R. Behanan, P. M. Davulis, D. Frankel, G. Bernhardt, T. Pollard and D. F. McCann, “Recent advances in harsh environment acoustic wave sensors for contemporary applications,” in *Proc. IEEE Sensors*, 2011, pp. 614-617.
- [3] T. Aubert, J. Bardong, O. Elmazria, G. Bruckner and B. Assouar, “Iridium interdigital transducers for high-temperature surface acoustic wave applications,” *IEEE Trans. Ultrason. Ferroelectr. Freq. Control*, vol. 59, no. 2, pp. 194-197, Feb. 2012.
- [4] T. Aubert, P. Nicolay, F. Sarry, “Thermoelastic effects in Pt IDTs. Impact on the behavior of high-temperature LGS-based SAW devices,” in *Proc. IEEE Ultrasonics Symp.*, 2013, pp. 259-262.
- [5] W.L. Goffe, G.D. Ferrier and J. Rogers, “Global optimization of statistical functions with simulated annealing,” *Journal of Econometrics*, vol. 60, pp. 65-99, 1994.
- [6] A. Bungo, C. Jian, K. Yamaguchi, Y. Sawada, R. Kimura and S. Uda, “Experimental and theoretical analysis of SAW properties of the langasite substrate with Euler angle $(0^\circ, 140^\circ, \theta)$,” in *Proc. IEEE Ultrasonics Symp.*, 1999, pp. 231-234.
- [7] J. Kräusslich, S. Höfer, U. Zastrau, N. Jeutter and C. Baehtz, “Temperature dependence of lattice parameters of langasite single crystals,” *Cryst. Res. Technol.*, vol. 45, no. 5, pp. 490-492, 2010.
- [8] P. Nicolay and T. Aubert, “A numerical method to derive accurate temperature coefficients of material constants from high-temperature SAW measurements. Application to langasite,” *IEEE Trans. Ultrason. Ferroelectr. Freq. Control*, vol. 60, no. 10, pp. 2137-2141, Oct. 2013.

- [9] J.J. Campbell and W.R. Jones, "A method for estimating optimal crystal cuts and propagation directions for excitation of piezoelectric surface waves," *IEEE Trans. Sonics Ultrason.*, vol. SU-15, pp. 209-217, 1968.
- [10] D.C. Malocha, M. Pereira da Cunha, E. Adler, R.C. Smythe, S. Frederick, M. Chou, R. Helmbold and Y.S. Zhou, "Recent measurements of material constants versus temperature for langatate, langanite and langasite," in *Proc. IEEE Int. Frequency Control Symp.*, 2000, pp. 200-205.
- [11] J. Hernando, J. L. Sánchez-Rojas, S. González-Castilla, E. Iborra, A. Ababneh and U. Schmid, "Simulation and laser vibrometry characterization of piezoelectric AlN thin films," *J. Appl. Phys.*, vol. 104, art. no. 053502, 2008.
- [12] P.M. Davulis and M. Pereira da Cunha, "A full set of langatate high-temperature acoustic wave constants: Elastic, piezoelectric, dielectric constants up to 900°C," *IEEE Trans. Ultrason. Ferroelectr. Freq. Control*, vol. 60, no. 4, pp. 824-833, Apr. 2013.